An integrated workflow centered around elastic FWI for complex subsalt imaging using wide-azimuth data in the southern Gulf of Mexico

Hongyan Li[2], Riaz Alai[1], Nolan Brand[2], Frederico Xavier de Melo[2], Hugo Enrique Muñoz Cuenca[2], Wenmiao Liu [2], Iestyn Williams[2], Saeeda Hydal[2], Khaled Abdelaziz[2], Emmi Sanchez Vargas[2], Nik Nur Halim C Soh[1], M Shah B Sulaiman[1]and Sandeep Kumar[1]*
1 – Petronas, 2 - SLB

Summary

Improving subsalt imaging quality and accuracy is the key to reduce exploration uncertainties in the Gulf of Mexico. The strategy proposed in this work significantly improved the subsalt image response, enabling the de-risking of deep prospects in the reimaging of legacy data acquired with a towed streamer wide-azimuth acquisition geometry. Considering the strong converted waves from salt and carbonate geometries, elastic FWI (EFWI) was employed to improve the subsalt velocity update. With the limitation of maximum offset and azimuth, a systematic workflow was proposed to improve subsalt velocity model building through converted wave velocity scanning, interleaved EFWI and tomography, and EFWI model guided salt scenario tests.

Introduction

The study area is located in the Campeche Bay, southern Gulf of Mexico (GoM). In this area, extensive compressional tectonics are evidenced, characterized by severe folding, deep-rooted thrusts, presence of complex allochthonous salt bodies, and rafted carbonate layers occurring at shallow, medium, and deep depths with associated variable geometries. The salt geometry is extremely complex with varying salt velocities due to salt sutures and sediment inclusions. These complex carbonate bodies, together with a pervasive shallow salt canopy, present a challenging subsalt imaging scenario in comparison to the northern GoM and other salt-dominated geological areas.

Considering the strong elastic effect from the salt and carbonate structures, elastic FWI (EFWI, Richardson et el., 2023) was applied in this project to improve the match between the seismic data and the predicted data, therefore, improving velocity inversion. However, the offsets of the wide-azimuth (WAZ) data in this project, defined by the 9-km cable length, limit the recorded diving wave penetration, directly impacting the effectiveness of EFWI at depth. Additionally, the WAZ data, acquired in 2015, has azimuth constraints relative to contemporary ocean-bottom-node (OBN) acquisition geometry. Due to these factors, common-image-point (CIP) tomography (Woodward et al., 2008) and manual salt adjustment testing were also included in the workflow to assist EFWI when resolving complex features at depth.

For EFWI, the Vp/Vs ratio was derived from several compressional (P) and shear (S) sonic logs near the study areas. Dual velocity salt flooding exercise was performed for P- and S-wave velocities through scanning and analysis of base salt event placement (Alai et al., 2006; Alai et al., 2022, Alai et al., 2023). The utilization of this technique helped defining the base salt geometries in comparison with P-only acoustic schemes, further improving the accuracy and convergency rate of the model building process. Additional imaging enhancement based on existing noise models and volumetric matching was done to further improve the primary response in the subsalt region.

In summary, EFWI integrated with CIP tomography and salt geometry adjustments based on FWI update, provided significant subsalt imaging improvement over legacy processing.

Method

Figure 1 shows the model building workflow used in this case study. The initial sediment model was obtained by revising the legacy sediment model based on better geological understanding acquired in recent years.

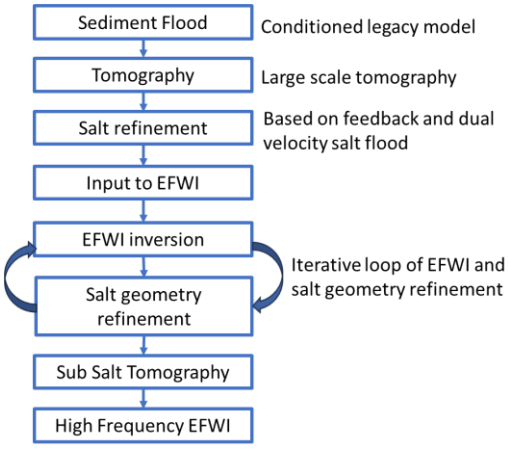

Figure 1: Modeling building workflow.

The sediment tomography was run to improve the model accuracy before EFWI to avoid potential cycle skipping for FWI. The salt horizons were adjusted from the legacy model based on salt flood of different components: PPPP, PSPP, PPSP, and PSSP. During the EFWI loop, the salt geometry was further adjusted based on the direction of the FWI update.

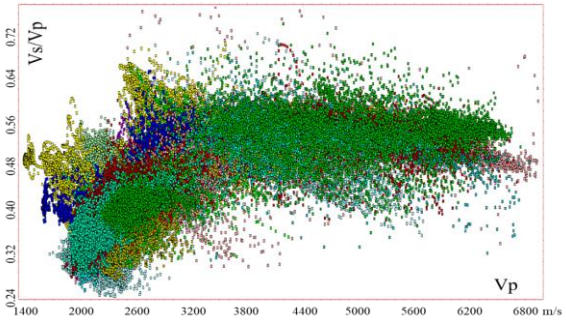

Figure 2: Vp vs. Vs/Vp ratio from sonics in nearby wells.

Figure 2 shows a cross plot of Vp vs. Vs/Vp from sonic logs in nearby wells. For the salt and other evaporites, the Vs/Vp is quite constant, ~0.57. For Vs/Vp in the clastic sediment, the relationship is derived as: Vs=Vp*0.7-723, based on Greenberg-Castagna Shale line (Sayers and Lennert, 2011).

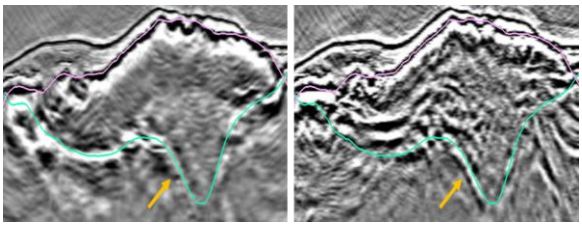

(a) (b)

Figure 3: P-wave (a) and S-wave (b) salt velocity flooding. The pink and green lines are interpreted top and base salt horizons. The P-wave salt velocity is 4480 m/s, and the Vs/Vp ratio is 0.57.

Figure 3 shows a salt flood RTM image with PPPP (a) and PSSP (b) velocity. The Vs/Vp salt velocity is defined as 0.57 by scanning a range of ratios. The consistency of the base salt from the P-wave and converted-wave images validated the ratio adopted for EFWI.

By comparing Figure 4(a) and 4(b), we can perceive positive image response from the initial to the EFWI model, more subsalt events are imaged with stronger amplitude. The large subsalt improvement areas are below large salt velocity change as pointed by yellow, blue and white arrows. However, we can still observe the undulation or discontinuity of the events as pointed by orange arrows.

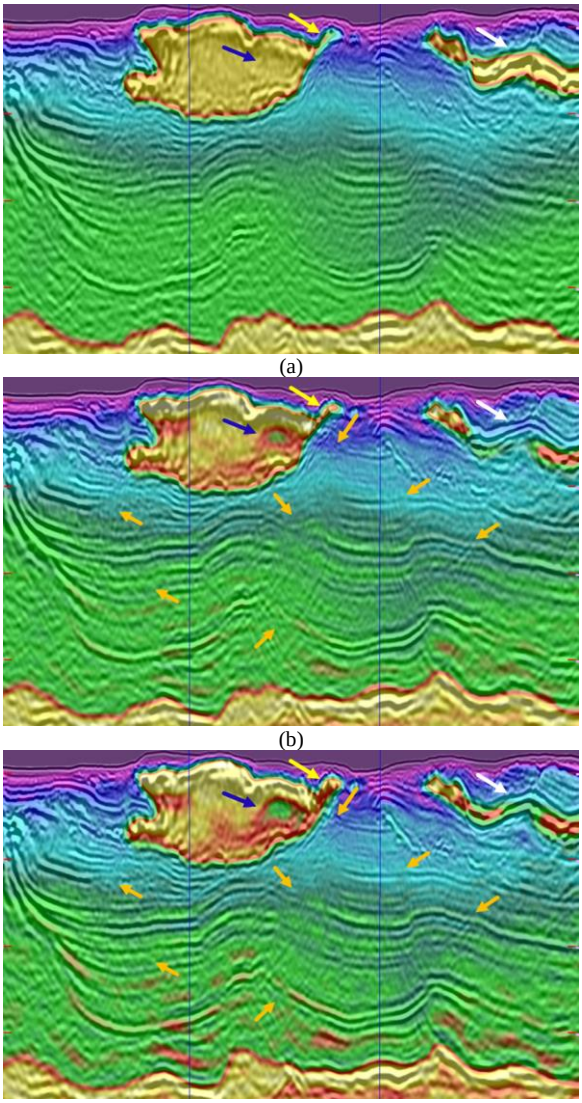

(a) (b) (c)

Figure 4: (a) EFWI initial velocity overlaid with RTM image; (b) EFWI updated velocity overlaid with RTM image; (c) EFWI updated velocity overlaid with RTM image incorporated with salt adjustment. The blue lines indicate full-fold data coverage area with 10-km aperture. The orange arrows point to different subsalt events. The yellow, blue, and white arrows indicate large salt velocity change after FWI.

Based on the FWI velocity update, sediment inclusion was interpreted in the blue arrow area, thicker salt was added in the salt wing (Yellow arrow), and the salt was revised to be lower-velocity carbonate in white arrow area. Further subsalt improvements are noted when incorporating these salt geometry adjustments (Figure 4c). The subsalt evets become more continuous and coherent comparing to 4(b). In this

case, the EFWI update was able to provide considerable assistance on salt interpretation, which in turn, helped EFWI convergence.

Figure 5 demonstrated the contribution of CIP tomography to the velocity update on top of EFWI. With more accurate velocity update in the shallow depth from EFWI, CIP tomography provided most update in the deeper session (below 6 km, Figure 5c). The deep subsalt events and base of Louann (Blue arrows) are better imaged with the model after tomography.

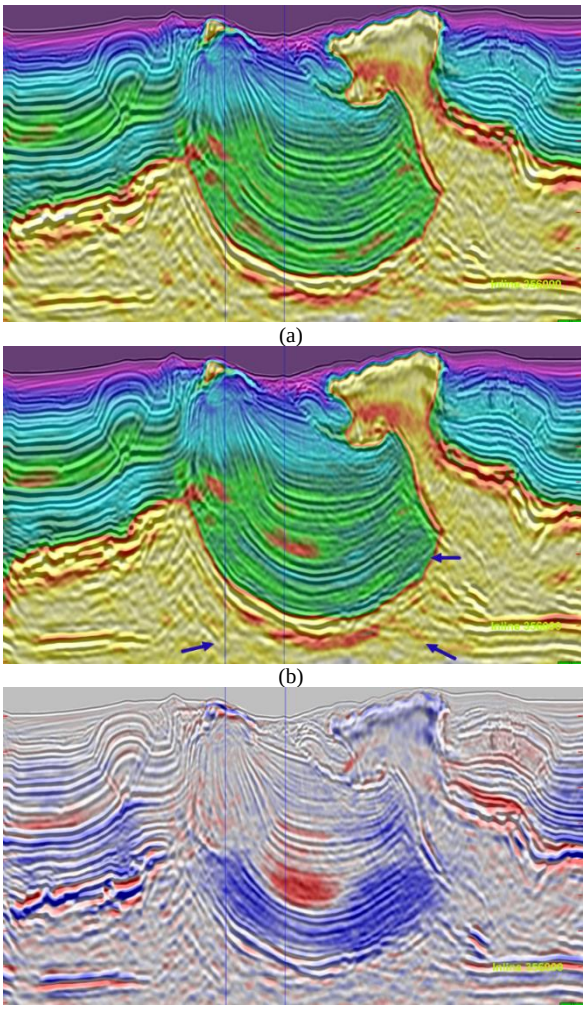

(a)

(b)

(c)

Figure 5: CIP tomography update. (a) Tomography input velocity overlaid with 12-Hz RTM image; b) Tomography output velocity overlaid with 12-Hz updated RTM image; (c) Tomography DV overlaid with updated 12-Hz RTM image. The blue lines indicate full-fold data coverage area with 10-km aperture.

Post-imaging enhancement was performed after the full construction of the earth model to attenuate residual coherent noise that interferes subsalt primary response, manifesting as strong crosstalk after migration. Simultaneous volumetric subtraction was applied in this case study to remove the residual surface multiples and other events, such as converted-wave noise and internal multiples, observed in complex subsalt regions. This approach was able to suppress most of the residual noise persistent in the raw image after migration, improving the image response near base of salt and subsalt regions, along with other places with strong noise contamination.

Examples

Figure 6 compares the final reprocessed RTM image with the legacy one. With volumetric subtraction, the converted wave (pointed by the red arrow), the residual surface multiples and other coherent noise (Indicated by the orange arrows) in 6a are very well attenuated in 6b. Higher signal-to-noise ratio is observed on the enhanced image. With the improved velocity model from EFWI together with CIP tomography, the subsalt image is recovered, more coherent events are imaged with stronger and consistent amplitude, especially the steep-dip events immediately below the thin salt, reducing the interpretation uncertainty in the subsalt region. The base of Louann salt becomes flatter and continuous (The deep event pointed by yellow arrows), indicating a more accurate subsalt velocity model. Compared to the legacy image in Figure 6c, the subsalt image is substantially improved by the reprocessing of WAZ data with EFWI integrated with salt adjustment and CIP tomography, especially in the circled area.

Conclusions

Within the constraints imposed by the towed-streamer WAZ acquisition geometry used to acquire this data, we presented an integrated workflow of EFWI, FWI driven salt scenario testing and CIP tomography, which yielded a vast improvement over the initial FWI and legacy velocity models and seismic images. Utilizing dual salt velocity migration, three additional images (PPSP, PSPP, and PSSP) were generated to help define the base of salt geometries in comparison with P-only acoustic schemes. In all, the combination of accurate earth model building and enhanced subsalt image helped derisking interpretation and potential subsalt prospects in the southern GoM.

Acknowledgement

We thank SLB Multiclient for the permission to use the data and our colleagues involved in processing the project.

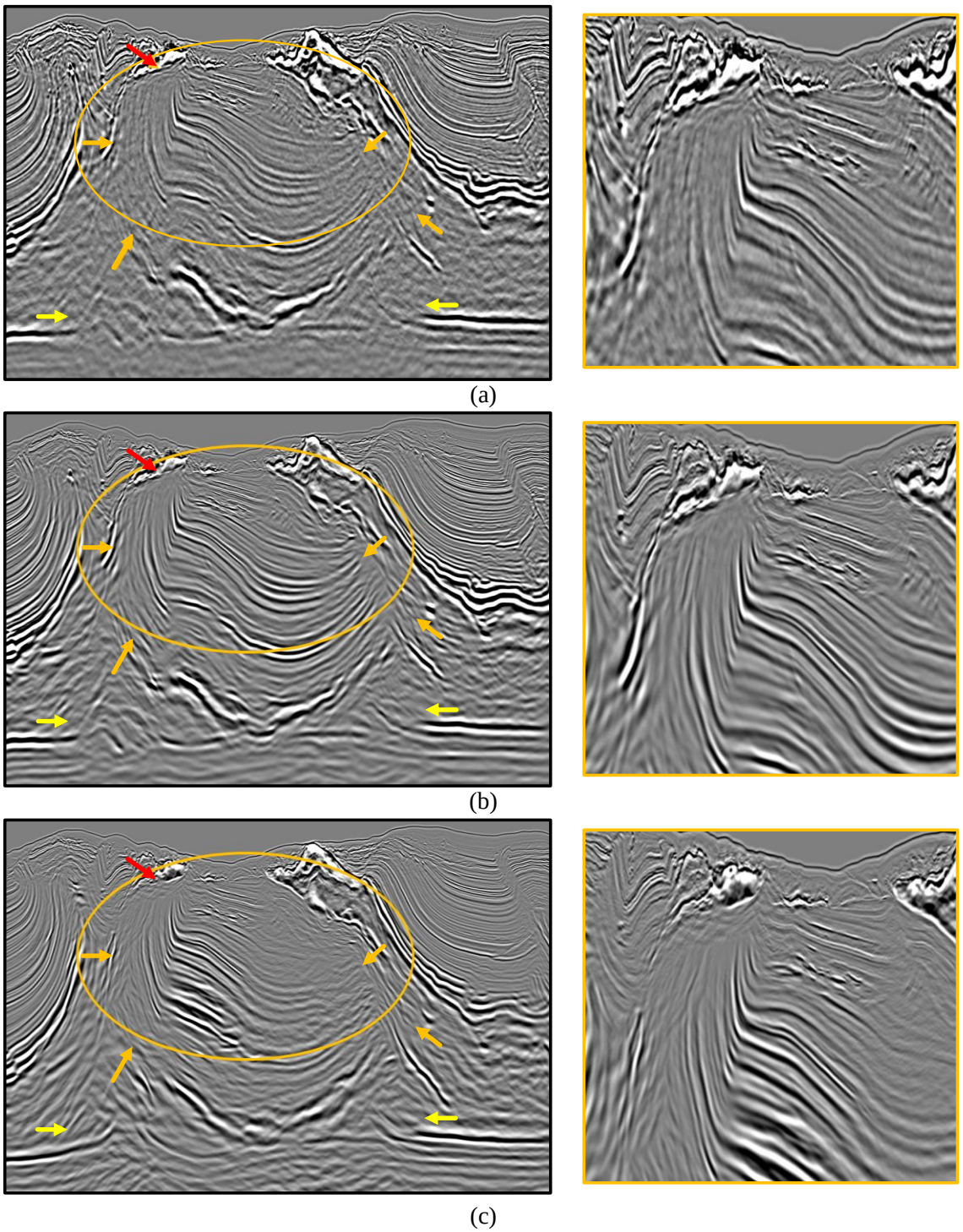

Figure 6. (a) Final 18-Hz raw RTM image; (b) Enhanced final 18-Hz RTM; (c) Legacy final enhanced 18-Hz RTM. The coherent noise pointed by the orange arrows on raw RTM are attenuated on the enhanced image. Highlighted sections on the right show visible improvements in (a) and (b) in comparison with the legacy outcome in (c).